An active contour framework based on the Hermite transform for shape segmentation of cardiac MR images

Leiner Barba-J*, Boris Escalante-Ramírez

Universidad Nacional Autónoma de México, Facultad de Ingeniería, C.U., México, D.F
Lab. Avanzado de Procesamiento de Imágenes, Edif. T, Posgrado en Ingeniería, 2do Piso

ABSTRACT

Early detection of cardiac affections is fundamental to address a correct treatment that allows preserving the patient's life. Since heart disease is one of the main causes of death in most countries, analysis of cardiac images is of great value for cardiac assessment. Cardiac MR has become essential for heart evaluation. In this work we present a segmentation framework for shape analysis in cardiac magnetic resonance (MR) images. The method consists of an active contour model which is guided by the spectral coefficients obtained from the Hermite transform (HT) of the data. The HT is used as model to code image features of the analyzed images. Region and boundary based energies are coded using the zero and first order coefficients. An additional shape constraint based on an elliptical function is used for controlling the active contour deformations. The proposed framework is applied to the segmentation of the endocardial and epicardial boundaries of the left ventricle using MR images with short axis view. The segmentation is sequential for both regions: the endocardium is segmented followed by the epicardium. The algorithm is evaluated with several MR images at different phases of the cardiac cycle demonstrating the effectiveness of the proposed method. Several metrics are used for performance evaluation.

Keywords: Cardiac MR Images, Segmentation, Active Contour, Hermite Transform

1. INTRODUCTION

Heart diseases constitute some of the major causes of death in developed and developing countries[1]. Early detection of cardiac affections is fundamental to address a correct treatment that allows preserving the patient's life. In this sense, Cardiac MR has become essential for heart evaluation. It consists of a noninvasive test that creates a set of image slices that code morphological, functional and metabolic information of the organs[2]. Thanks to current technologies, MR tests can also provide information of the complete cardiac phases of the heart. Several heart failures and conditions can be diagnosed with MRI including coronary artery disease, affections provoked by heart attacks, problems of the valves, heart muscle disease, congenital defects and others[2].

Among the cardiac structures, the left ventricle is of main interest for the detection of heart failures using MR tests[3-4]. Several cardiopathies can be diagnosed through with evaluation of the left ventricle size at both end-diastolic (ED) and end-systolic (ES) phases[5]. Left ventricle mass is also an important parameter used as a predictor of morbidity and mortality in some patients[6]. The evaluation of these structures implies a previous segmentation using any of the cardiac image modality. In this work we focus our attention on the MR modality. Because manual segmentation is a tedious and time consuming task that mostly depends on the observer, automatic algorithms became very helpful tools for shape extraction and cardiac evaluation. Inter and intra-observer variations presented in manual segmentations of cardiac structures are enough reasons for seeking more stable and objective heart evaluations supported on automatic or semi-automatic algorithms.

*lebaji@gmail.com

Optics, Photonics and Digital Technologies for Imaging Applications IV, edited by Peter Schelkens, Touradj Ebrahimi, Gabriel Cristóbal, Frédéric Truchetet, Pasi Saarikko, Proc. of SPIE Vol. 9896, 98960U · © 2016 SPIE · CCC code: 0277-786X/16/$18 · doi: 10.1117/12.2223450

Segmentation of the left ventricle using MR images is a problem that researches have tried to solve for many years. Although many algorithms have been proposed, this problem still remains as an open issue[3]. One cause is the lack of a huge database that can be used for comparison purposes among the community of researchers. In this sense, a collaborative project has been already initiated with the aim of building a platform that allows proving and comparing segmentation algorithms[7]. Nonetheless, a public database of cardiac MR images is available for research purposes: the MICCAI database used at the 2009 challenge[8]. We used this data in our work to validate the proposed segmentation algorithm.

Generally speaking, segmentation of cardiac MR images is not an easy task. Low contrast, shape variations and diffuse edges are the most frequently problems found in cardiac MR images. Including papillary muscles as part of the left ventricle cavity constitutes a great challenge for segmentation algorithms[4]. Two regions are of main interest when segmenting the left ventricle: endocardium and epicardium. The latter is of greater difficulty since the contrast between the myocardium and surrounding tissues is very poor. Probabilistic algorithms[9], parametric[10] and implicit[11] active contours, and trained approaches[12] have been designed to deal with these problems.

Needless to say, segmentation based on active contours is among the most accepted processing techniques for medical image applications. It consists of evolving curves guided by internal and external forces that may depends on the image characteristics. These forces are designed to stop the evolution of the curves at the object boundaries. With active contours the segmentation process is commonly modeled as a functional equation that could include different types of terms: boundary and region-based forces, or combination of both forces[13]. Implicit active contours which are represented using level sets have many advantages regarding implementation, extension to several dimensions and facility to combine different forces. Moreover, changes of configuration are assumed naturally by the curves.

Due to the fact that evolution in active contour models is guided by velocities that mostly depends on images features, we must find an efficient way to extract this information. The Hermite transform (HT) is an interesting mathematical tool used for coding image characteristics[14]. It decomposes an image using the set of orthonormal functions composed by the Hermite polynomials. Computing of directional edges, noise reduction and texture coding can be competently achieved with the HT. Several works have demonstrated the capability of the HT for coding data in different applications[15]. In this work we propose a segmentation framework applied to left ventricle in cardiac MR images. An active contour that combines edge, region and geometrical velocities is used. Coefficients of the HT allow codification of the two first velocities. Our algorithm is evaluated on several cardiac MR images obtained from the MICCAI challenge database[8].

The rest of the paper is organized as follows. The proposed algorithm is described in section 2: the HT and the proposed active contour are described. Section 3 presents evaluations and experimental results. Conclusion and discussion are presented in section 4.

2. METHODOLOGY

We designed an implicit active contour with four velocity terms for segmenting the endocardial and epicardial boundaries. The segmentation is sequential for both regions: the endocardium is segmented followed by the epicardium. Let $C = \big(X(s)\big), X \in R^2$ be a parametric moving interface that fragments the image domain Ω into two regions. This interface can be represented as the zero level set of a higher dimensional function, $C = \varphi(X(s)) = 0$. The following convention for the level set function is used: $\varphi(X(s)) < 0$ for $X(s)$ inside C, $\varphi(X(s)) > 0$ for $X(s)$ outside C and $\varphi(X(s)) = 0$ for $X(s)$ in C. A sign distance function is also used to represent the level set function. The general proposed energy functional using a level set framework is written as follows:

$$E(m_1, m_2, \varphi_s, \varphi) = \lambda_1 E_D(m_1, m_2, \varphi) + \lambda_2 E_B(\varphi) + \lambda_3 E_S(\varphi_s, \varphi) + \lambda_4 E_R(\varphi) \quad (1)$$

where E_D is the region term, E_B is the boundary term, E_S is the shape term and E_R is the regularization term. Region and boundary terms are directly computed from the image data while shape and regularization terms are based on the interface or level set function. Weight parameters $\lambda_m, m = 1, \ldots, 4$ control the contribution of each term. We used the HT for image data computing. Each term of the functional as well as the HT are shortly described below.

2.1. The Hermite transform

As any other transform, with the HT we aim at projecting the image onto a set of functions in order to better code image features. In this transform the set of orthonormal functions composed by the Hermite polynomials is used for image projection[14]. Let $f(x,y)$ be an arbitrary function, its HT consists of a windowed operation whose coefficients $L_{m,n-m}(p,q)$ are calculated as follows:

$$L_{m,n-m}(p,q) = \iint_{-\infty}^{\infty} f(x,y)V^2(x-p,y-q)G_{m,n-m}(x-p,y-q)dxdy \quad (2)$$

where $V(x,y) = \left(\frac{1}{(\sigma\sqrt{\pi})^2}e^{-(x^2+y^2)/\sigma^2}\right)$ is a Gaussian window centered at (p,q) and $G_{m,n-m}(x,y) = \frac{1}{\sqrt{2^n(n-m)!n!}}H_{n-m}(x/\sigma)H_m(y/\sigma)$ are the set of orthonormal Hermite polynomials. Coefficients are defined for $n = 0,1,2,\dots,N$ and $m = 0,1,\dots,n$ where n is the order of the transformation. The HT can be computed as the convolution of the input function $f(x,y)$ and the Hermtie filters defined as $D_{m,n-m}(x,y) = V^2(-x,-y)G_{m,n-m}(-x,-y)$, followed by a dowsampling process at the (p,q) positions. Although the HT has been of main interest in several fields, the potential of this tool remains unexplored in medical applications. Many advantages distinguish the HT from other similar mathematical tools: orthogonality property, continuous and discrete definitions, base of separable functions, it is not critically sampled and the possibility to perform multiscale/multiresolution processing[16]. Hermite coefficients are arranged using the graphical scheme depicted in Figure 1a. An example of the HT computed for a cardiac MR image is illustrated in figure 1b. Coefficients are shown until order $n = 2$. Each coefficient of the HT codes different features of the analyzed image. The coefficient of order $n = 0$ is a smoothed version of the original image, coefficients of order $n = 1$ respresents the edge of the image and coeffiecients of order $n > 1$ are suitable for texture analysis.

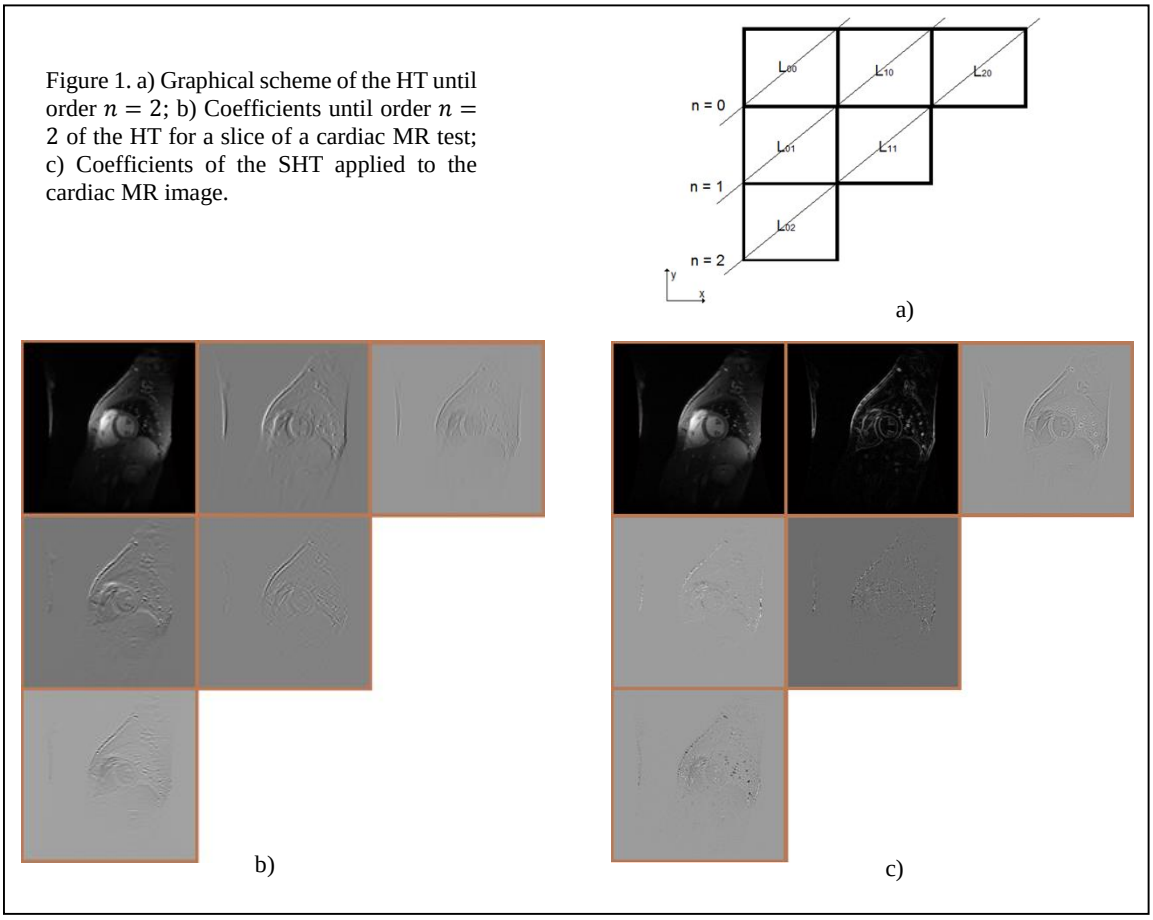

Figure 1. a) Graphical scheme of the HT until order $n = 2$; b) Coefficients until order $n = 2$ of the HT for a slice of a cardiac MR test; c) Coefficients of the SHT applied to the cardiac MR image.

Hermite filters, on the other hand, ensemble a set of Gaussian derivative functions which are commonly known to be very efficient for directional processing[17]. This latter property has permitted the definition of the Steered Hermite transform (SHT) which is an efficient and powerful tool for local orientation analysis[16]. With the SHT, the Cartesian coefficients obtained with equation (2) can be steered using a linear combination of them. The importance of the SHT lies on the fact that several image patterns, such as edges and texture, should be better analyzed using directional functions. We recommend readers to review[16, 18] for further analysis regarding the STH. In this work we used the SHT for image data processing. Figure 1c shows the SHT coefficients of the example depicted in figure 1b. Here, we can see that most of the energy of the coefficients is concentrated in the first row of the scheme.

2.2. Region term

We adopted the region energy proposed by the Chan-Vese model[19]. This consists of a global term which assumes that regions of the image inside and outside the active contour are characterized by two constant functions. The functional describing this term is written using the level set framework as follows:

$$E_D(m_1, m_2, \varphi) = \int_\Omega (I - m_1)^2 H\big(\varphi(X)\big) dX + \int_\Omega (I - m_2)^2 \Big(1 - H\big(\varphi(X)\big)\Big) dX \quad (3)$$

where m_1 and m_2 are the functions which characterize regions inside and outside the interface respectively. They are computed as the average of the intensity values of each region. I is the input image used to calculate the global parameters m_1 and m_2. For this image we used the coefficient of order $n = 0$ of the SHT, it means $I = L_{0,0}$. The level of smoothing is controlled in the SHT with the scale parameter of the Gaussian window V. For minimization purposes, level set functions are usually represented using Heaviside $H(z)$ and Delta Dirac $\delta(z)$ functions[19], regularized as: $H_\varepsilon(z) = \frac{1}{2}\left(1 + \frac{2}{\pi} tan^{-1}\left(\frac{z}{\varepsilon}\right)\right)$ and $\delta(z) = \frac{d}{dz}\big(H(z)\big)$. For the endocardial segmentation, the blood pool of the left ventricle cavity is the region inside the contour. In the epicardial segmentation, the left ventricle cavity is removed and then the myocardium constitutes the inside region.

2.3. Boundary term

Boundary terms are based on edge descriptor functions. The goal of this term is to stop the evolution of the interface at the edge of the objects. We used the functional proposed in[20] for the boundary term. This functional is expressed as follows:

$$E_B(\varphi) = \int_\Omega g H\big(\varphi(X)\big) dX \quad (4)$$

where $g = \frac{1}{1+IE}$ is a function that approximates zero at the edge of the objects[21]. IE is the edge map of the input image. The coefficient $L_{1,0}$ of the SHT is used as edge map in this functional. One of the principal causes of failure for edge-based segmentation algorithms is the presence of intensive noise in the images. This requires of robust filtering algorithms that may help to identify the correct boundaries. With SHT the cartesian coefficients are steered following the maximum energy direction for each pixel. Since noise is not directional, it can be removed by simply using this steering operation.

2.4. Shape term

Medical images are frequently processed using geometrical models. The use of shape parameters in level set frameworks help to settle segmentation problems of the papillary muscles. It is accepted that papillary muscles are considered to be part of the left ventricle cavity for clinical measurements[22]. Left ventricle in MR images also presents poor contrast and subtle edges in several parts of the region of interest which justifies the design of shape-based functionals. In these cases the shape parameter is fundamental to control the deformation of the active contour. In left ventricle segmentation approaches, it is common to assume that endocardial and epicardial boundaries can be described using circular or elliptical shapes[10, 23]. Other researches prefer using trained shape models to statistically learn the geometrical properties of the shapes[24]. However, a disadvantage of previously trained methods is that they require a huge database of shape samples[25].

In this work, we follow the assumption that an ellipse describes the left ventricle shape[23], unlike we adopted the following shape functional which is similar to that exposed in [26]:

$$E_S(\varphi_s, \varphi) = \int_\Omega \left(\varphi(X) - \varphi_s(X)\right)^2 H\big(\varphi(X)\big) dX \tag{5}$$

where φ_s is the prior shape assumed. As can be seen, this prior shape consists of a sign distance function which is compared to the level set function. In order to build φ_s, we need to estimate the ellipse that better fit the current contour. A simple but an effective method is used for ellipse estimation[27]. In contrast to last energy functions, the shape term does not depend on the image features.

2.5. Regularization term

Under the idea that good segmentations should have smooth and short contours, it is usual to penalize the length of the zero level set through with a regularization term[19]. The following functional is the standard regularization term used for level set based segmentation methods:

$$E_R(\varphi) = \int_\Omega \left|\nabla H\big(\varphi(X)\big)\right| dX = \int_\Omega \delta\big(\varphi(X)\big) |\nabla \varphi(X)| dX \tag{6}$$

where ∇ is the gradient operator. Similar to the shape functional, the regularization term only depends on the level set function, i.e., it is a geometrical parameter as well.

2.6. Minimization of the energy functional

The complete energy functional proposed in this work is the weighted combination of all the energy terms described above. For simplicity we change $\varphi(X)$ as φ, therefore:

$$E(m_1, m_2, \varphi_s, \varphi) = \lambda_1 \left(\int_\Omega (I - m_1)^2 H(\varphi) dX + \int_\Omega (I - m_2)^2 \left(1 - H(\varphi)\right) dX \right) + \lambda_2 \int_\Omega g H(\varphi) dX + \lambda_3 \int_\Omega (\varphi - \varphi_s)^2 H(\varphi) dX + \lambda_4 \int_\Omega \delta(\varphi) |\nabla \varphi| dX \tag{7}$$

The minimization process is addressed in two stages. In the first one φ is fixed while m_1, m_2 and φ_s are computed. In the second stage the energy functional is minimized for φ. Using the calculus of variation and the gradient descent method, the evolution equation that minimizes E is written as:

$$\frac{\partial \varphi}{\partial t} = \left(\lambda_1 ((I - m_2)^2 - (I - m_1)^2) + \lambda_2 g + \lambda_4 div\left(\frac{\nabla \varphi}{|\nabla \varphi|}\right) \right) \delta(\varphi) - 2\lambda_3 H(\varphi)(\varphi - \varphi_s) \tag{8}$$

The evolution of the final equation is iterative. An initial approximate φ_0 of the segmentation is needed. A maximum number of iterations is used to stop the contour evolution. We implemented the narrow band strategy to optimize processing time.

3. EXPERIMENTS AND RESULTS

In this section we present the experiments and preliminary results of the designed algorithm. Eight patients were used to validate the segmentation approach. They were taken from the MICCAI challenge database which consists of MR short axis images acquired with a 1.5T GE Signa MRI. The complete set of images were obtained during 10-15 second breath-holds with a temporal resolution of 20 cardiac phases over the heart cycle, and scanned from the ED phase[8]. Each volume of the cardiac cycle consists of 6-12 slices acquired from base to apex. Individual slices were used for evaluation. Ground truth for endocardial boundary at the End-Systolic (ES) phase, and for epicardial and endocardial boundaries at the End-Diastolic (ED) phase are provided.

Two metrics were used in this work to validate the segmentation framework. A point to curve distance is employed to compare the contours of the segmentation against the ground truth. Table 1 describes the results of the segmentation using the distance metric computed for the eight patients. We average the distance computed for all the slices that composes the heart from base-to-apex.

Table 1. Distance between the segmented contours and the ground truth. The distance is expressed in mm (mean ± std).

Patient	**Endocardium**		**Epicardium**
	ED Contour	*ES Contour*	*ED Contour*
P1	3.2550 ± 0.5125	2.6924 ± 0.2803	2.7358 ± 0.4639
P2	3.0603 ± 0.9292	3.1186 ± 0.6748	3.5392 ± 0.5218
P3	2.7891 ± 0.7274	2.8404 ± 0.6977	2.2948 ± 0.2653
P4	2.7113 ± 0.3239	2.8179 ± 0.3158	3.1150 ± 0.3887
P5	2.8011 ± 0.4446	3.2922 ± 0.5961	3.6289 ± 0.4590
P6	2.4307 ± 0.4796	2.7198 ± 0.3474	2.4436 ± 0.7758
P7	3.8397 ± 0.6383	4.5013 ± 0.5270	5.0080 ± 0.7344
P8	4.5433 ± 0.5740	4.3081 ± 0.3637	4.9088 ± 0.1759

Dice similarity coefficient (DSC) is the other metric used in this work to evaluate the segmentation performance. Figure 2 shows bar diagrams with the DSC calculated for endocardial and epicardial areas resulted from the segmentation at the ED phase.

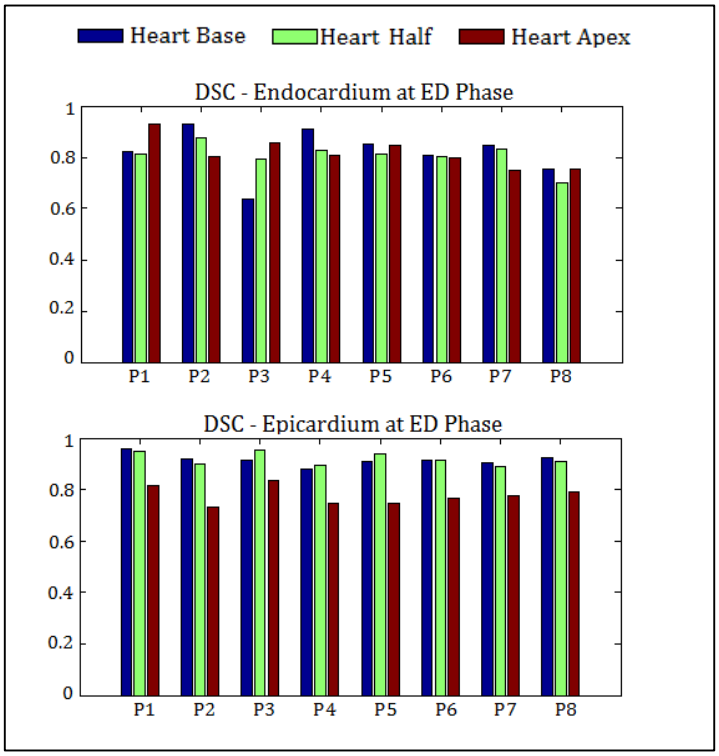

Figure 2. DICE analysis for eight MRI studies. The DSC is computed for three slices at the ED phase. Analysis for the endocardium and epicardium of the left ventricle are shown.

Figures 3 and 4 illustrates several contours obtained with our segmentation approach compared against the manual annotation. Results for two patients are shown. Images of the left ventricle at the base, half and apex of the heart are analyzed. The red contour is the ground truth and the blue contour is the segmentation obtained with the proposed framework. In figure 3, the segmentation is depicted for images at the ES phase while in figure 4 the segmentation is

shown for images at the ED cycle. The endocardium is only segmented for the ED phase while both regions are segmented in the ES phase. It can be seen that good segmentations are reached in these two cases. A Similar behavior is obtained for the rest of the patients.

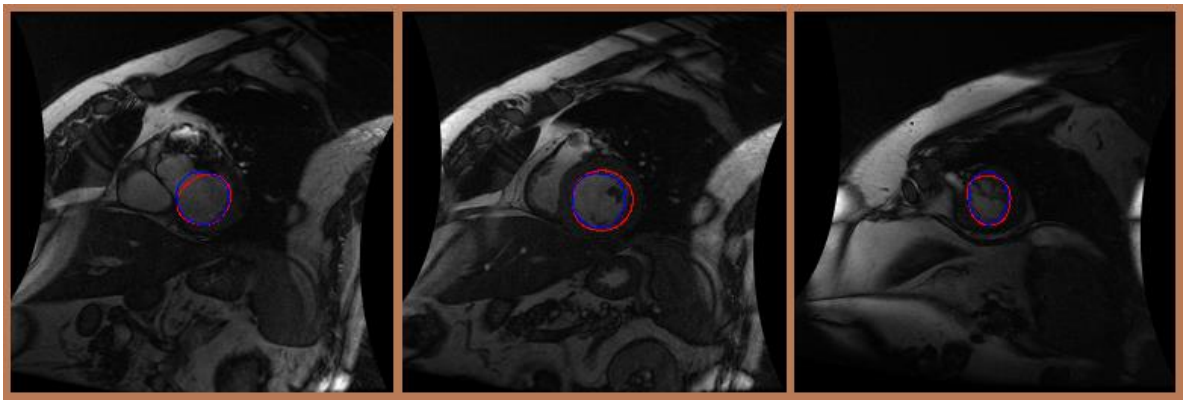

a) b) c)

Figure 3. Endocardial segmentation using the automatic proposed algorithm (blue contour) and the expert annotation (red contour) at the a) Base, b) Half and c) Apex of the heart. The images were acquired at the ES phase.

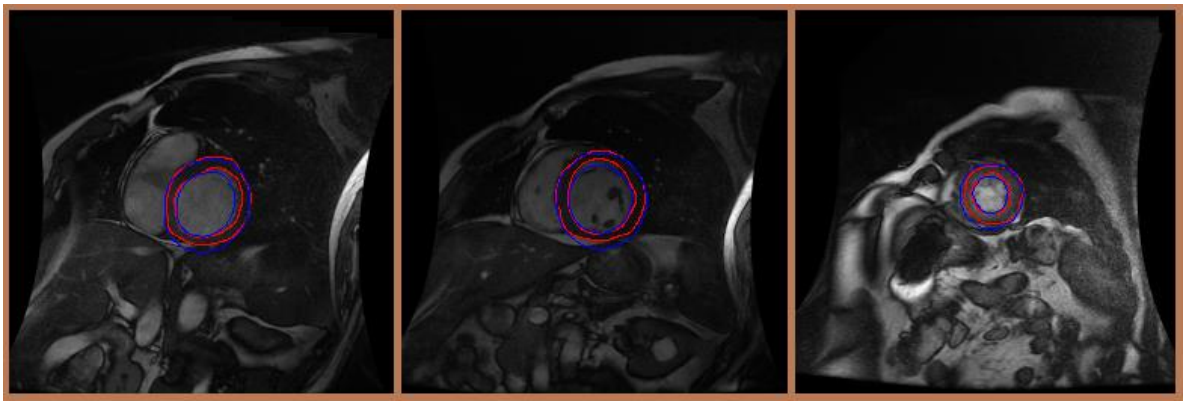

a) b) c)

Figure 4. Endocardial and epicardial segmentation using the automatic proposed algorithm (blue contour) and the expert annotation (red contour) at the a) Base, b) Half and c) Apex of the heart. The images were acquired at the ED phase.

4. DISCUSSIONS AND CONCLUSIONS

From the results described in table 1, we can see that the distance metric computed between the segmented contour and the manual annotation is under 5mm in most of the cases. The epicardial segmentation presents worse results compared to the endocardial segmentation. This is due to the irregularity of the intensities that surround the myocardium. Designing a functional that is able to deal with these problems is most complicated. The lack of edges and the variability of the intensities in some parts of the epicardium boundary make more difficult the segmentation task. "Leaking" problems of the contour in the epicardial boundary are almost controlled with the shape energy, which also allows including the papillary muscle as part of the left ventricle cavity. Figures 3 and 4 at the half part of the heart illustrate this behavior.

DICE analysis in figure 2 illustrates the behavior of the designed algorithm in three parts of the heart: base, half and apex. It can be seen that apex is the most difficult region to be segmented. The lack of information, subtle edges and irregularity of the left ventricle are the principal causes of the segmentation errors. These problems are more evident in the ES phase. In the base of the heart there are connected components to the left ventricle cavity that present similar intensity values. The shape energy avoids the contour to be propagated through this region, see figure 3a.

The Hermite coefficients used as input data for the energy functional in our level set method provide advantages regarding noise reduction and better edge detection. The steered property of the Hermite transform allows concentrating most of the energy in less coefficients. Local directional analysis of the data can be then addressed.

In this work we have introduced a segmentation method applied to cardiac MR images for the analysis of the left ventricle. The method is based on an active contour guided by the Hermite coefficients and two geometrical parameters. Four energy terms compose the proposed level set approach. Eight patients of the MICCAI database and two metrics were used for validation. Results of the segmentation illustrate good general performance of the proposed framework.

ACKNOWLEDGEMENTS

This work has been sponsored by the following UNAM grant: PAPIIT IG100814. Leiner Barba-J thanks CONACYT–245976 for financial support.

REFERENCES

[1] Cheung, Y. f., "The role of 3D wall motion tracking in heart failure," Nature Reviews Cardiology 9(11), 644-657 (2012).
[2] Yicheng, N., [MR Contrast Agents for Cardiac Imaging, In: Jan Bogaert, Steven Dymarkowski, Andrew M. Taylor, Vivek Muthurangu. Clinical Cardiac MRI, Medical Radiology/Diagnostic Imaging], Springer Science & Business Media, New York, 31 (2012).
[3] Petitjean, C., Dacher, J.N., "A review of segmentation methods in short axis cardiac MR images," Medical Image Analysis 15(2), 169-184 (2011).
[4] Kang, D., Woo, J., Slomka, P. J., Dey, D., Germano, G., and Jay Kuo, C. C., "Heart chambers and whole heart segmentation techniques: review," Journal of Electronic Imaging 21(1), 010901 (2012).
[5] William, H. G. and William, C. L., "Assessment of Left Ventricular Diastolic Function and Recognition of Diastolic Heart Failure," Circulation 116, 591-593 (2007).
[6] Mor-Avi, V., Sugeng, L., Weinert, L., MacEneaney, P., Caiani, E. G., Koch, R., Salgo, I. S., Lang, R. M., "Fast measurement of left ventricular mass with real-time three-dimensional echocardiography: comparison with magnetic resonance imaging," Circulation 110, 1814-1818 (2004).
[7] Suinesiaputra, A., Cowan, B. R., Al-Agamy, A. O., Elattar, M. A., Ayache, N., Fahmy, A. S., Khalifa A. M., Medrano-Gracia, P., Jolly, M. P., Kadish, A. H., Lee, D. C., Margeta J., Warfield, S. K., Young, A. A., "A collaborative resource to build consensus for automated left ventricular segmentation of cardiac MR images" Medical Image Analysis 18, 50-62 (2014).
[8] Suinesiaputra, A., Cowan, B., Finn, J., Fonseca, C., Kadish, A., Lee, D., Medrano-Gracia, P., Warfield, S., Tao, W., Young, A., "Left ventricular segmentation challenge from cardiac MRI: a collation study," Proc. Statistical Atlases and Computational Models of the Heart. Imaging and Modelling Challenges LNCS 7085, 88-97 (2012).
[9] Sénégas, J., Cocosco, C., Netsch, T., "Model-based segmentation of cardiac MRI cine sequences: a bayesian formulation," Proc. SPIE 5370, 432-443 (2004).
[10] Wu, Y., Wang, Y., Jia, Y., "Segmentation of the left ventricle in cardiac cine MRI using a shape-constrained snake model," Computer Vision and Image Understanding 117(9), 990-1003 (2013).
[11] Woo, J., Slomka, P. J., Jay Kuo, C. C., Byung-Woo, H., " Multiphase segmentation using an implicit dual shape prior: Application to detection of left ventricle in cardiac MRI," Computer Vision and Image Understanding 117 (9), 1084-1094 (2013).
[12] Barba-J, L., Olveres, J., Escalante-Ramírez, B., Arámbula, F. and Vallejo, E., "Segmentation of 4D cardiac computed tomography images using active shape models," Proc. SPIE 8436, 84361E (2012).
[13] Cremers, D., Rousson, M., and Deriche, R., "A Review of Statistical Approaches to Level Set Segmentation: Integrating Color, Texture, Motion and Shape," International Journal of Computer Vision 72(2), 195-215 (2007).
[14] Martens, J. B., "The Hermite transform - theory," IEEE Transactions Acoustics Speech and Signal Processing 38(9), 1595-1606 (1990).
[15] Martens, J. B., "The Hermite transform: A survey," EURASIP Journal on Advances in Signal Processing 2006, 1-20 (2006).

[16] Silván-Cárdenas, J. L. and Escalante-Ramírez, B., "The Multiscale Hermite Transform for Local Orientation Analysis," IEEE Transactions on Image Processing 15(5), 1236-1253 (2006).
[17] Freeman, W. T., Adelson, E. H.; "The Design and Use of Steerable Filters," IEEE Transactions on Pattern Analysis and Machine Intelligence 13(9), 891-906 (1991).
[18] Martens, J. B., "Local orientation analysis in images by means of the Hermite transform," IEEE Trans. Image Process. 6(8), 103-1116 (1997).
[19] Chan, T. and Vese, L., "Active contours without edges," IEEE Trans. Image. Process. 10(2), 266-277 (2001).
[20] Hsien-Chi, K., Giger M. L., Reiser, I., Drukker, K., Boone, J. M., Lindfors, K. K., Yang, K., Edwards, A. Sennett, C. A., "Segmentation of breast masses on dedicated breast computed tomography and three-dimensional breast ultrasound images," J. Med. Imag. 1(1), 014501 (2014).
[21] Caselles, V., Kimmel, R. and Sapiro, G., "Geodesic active contours," International Journal of Computer Vision 22(1), 61-79 (1997).
[22] Pednekar, A. S., Muthupillai, R., Cheong, B., Flamm, S. D., "Automatic computation of left ventricular ejection fraction from spatiotemporal information in cine-SSFP cardiac MR images," J. Magn. Reson. Imaging. 28(1), 39-50 (2008).
[23] Pluempitiwiriyawej, C., Moura, J. M. F., Wu, Y. J. L. and Ho, C., "STACS: New active contour scheme for cardiac MR image segmentation," IEEE Trans. Med. Imag. 24(5), 593-603 (2005).
[24] Rousson, M., and Cremers, D., "Efficient Kernel Density Estimation of Shape and Intensity Priors for Level Set Segmentation," Proc. International Conf. Medical Image Computing and Computer-Assisted Intervention 1, 757-764 (2005).
[25] Ben Ayed, I., Li, S. and Ross, I., "Embedding overlap priors in variational left ventricle tracking," IEEE Trans. Med. Imag. 28(12), 1902-1913 (2009).
[26] Rousson, M. and Paragios, N., "Shape Priors for Level Set Representations," Proc. ECCV LNCS 2351, 78-92 (2002).
[27] Rosin, P. L., "A note on the least squares fitting of ellipses," Pattern Recognition Letters 14(10), 799-808 (1993).